ADVANCED FUNCTIONAL MATERIALS
www.afm-journal.de

RGD-Conjugated Nanoscale Coordination Polymers for Targeted T_1- and T_2-weighted Magnetic Resonance Imaging of Tumors in Vivo

*Hong Yang, Changyuan Qin, Chao Yu, Yang Lu, Hongwei Zhang, Fengfeng Xue, Dongmei Wu, Zhiguo Zhou, and Shiping Yang**

Development of multifunctional nanoscale coordination polymers (NCPs) allowing for T_1- and T_2-weighted targeted magnetic resonance (MR) imaging of tumors could significantly improve the diagnosis accuracy. In this study, nanoscale coordination polymers (NCPs) with a diameter of ≈80 nm are obtained with 1,1′-dicarboxyl ferrocene (Fc) as building blocks and magnetic gadolinium(III) ions as metallic nodes using a nanoprecipitation method, then further aminated through silanization. The amine-functionalized Fc-Gd@SiO_2 NCPs enable the covalent conjugation of a fluorescent rhodamine dye (RBITC) and an arginine-glycine-aspartic acid (RGD) peptide as a targeting ligand onto their surface. The formed water-dispersible Fc-Gd@SiO_2(RBITC)–RGD NCPs exhibit a low cytotoxicity, as confirmed by MTT assay. They have a longitudinal relaxivity (r_1) of 5.1 mM^{-1} s^{-1} and transversal relaxivity (r_2) of 21.7 mM^{-1} s^{-1}, suggesting their possible use as both T_1-positive and T_2-negative contrast agents. In vivo MR imaging experiments show that the signal of tumor over-expressing high affinity $\alpha_v\beta_3$ integrin from T_1-weighted MR imaging is positively enhanced 47±5%, and negatively decreased 33±5% from T_2-weighted MR imaging after intravenous injection of Fc-Gd@SiO_2(RBITC)–RGD NCPs.

1. Introduction

By combining complementary diagnostic information obtained from various imaging methods, including X-ray computed tomography (CT), optical imaging, magnetic resonance (MR) imaging, positron emission tomography (PET), single-photon-emission computed tomography (SPECT) and ultrasound, multi-mode imaging techniques have been devised to offer more comprehensive diagnostic information and to study the dynamics of disease progression.[1] However, because of the different penetration depths and spatial/time resolutions of each imaging technology, it is still very difficult to coordinate the different imaging methods of a multi-mode imaging strategy. To address this problem, a multi-mode imaging technique on a single instrument should be developed.

MR imaging, a non-invasive imaging method based on the interaction of protons with the surrounding molecules of tissues, is one of the most powerful diagnostic techniques for living organisms.[2] The use of contrast agents can help to clarify images and allow better interpretation. The current MR imaging contrast agents are in the form of T_1-weighted positive agents[3] that can shorten longitudinal relaxation of protons, and T_2-weighted negative agents[4] that can shorten transverse relaxation of protons. Generally, a T_1-weighted image optimally shows the normal soft tissue anatomy such as fat, whereas a T_2-weighted image reveals pathological phenomena such as tumors and inflammation. Therefore, T_1/T_2 dual-mode MR imaging, which can provide complementary information, should attract considerable interest. Recently, Park and co-workers[5] and our group[6] respectively developed gadolinium (Gd) complex coated Fe_3O_4 nanoparticles for dual-mode T_1- and T_2-weighted MR imaging of tumors, respectively. Lu and co-workers[7] and Gao and co-workers[8] reported ultrasmall magnetic iron oxide and Gd_2O_3-embedded iron oxide nanoparticles as T_1-positive and T_2-negative dual-contrast agents, respectively. However, the conventional T_1/T_2 dual-mode contrast agents require multiple synthetic steps and additional costs to avoid convoluted behavior and effects in vivo and to clear substantial regulatory hurdles.

Alternatively, coordination polymers, which are generated from bridging ligands as linkers and metal ions as connectors, are a class of molecular inorganic/organic hybrid materials. They have been widely applied in chemistry, physics and related

Dr. H. Yang, C. Y. Qin, C. Yu, Y. Lu, H. W. Zhang, F. F. Xue, Z. G. Zhou, Prof. S. P. Yang
The Education Ministry Key Lab of Resource Chemistry & Shanghai Key Laboratory of Rare Earth Functional Materials
Shanghai Normal University
Shanghai 200234, China
E-mail: shipingy@shnu.edu.cn
D. M. Wu
Shanghai Key Laboratory of Magnetic Resonance
Department of Physics
East China Normal University
3663, North Zhongshan Road, Shanghai 200062, China

DOI: 10.1002/adfm.201302433

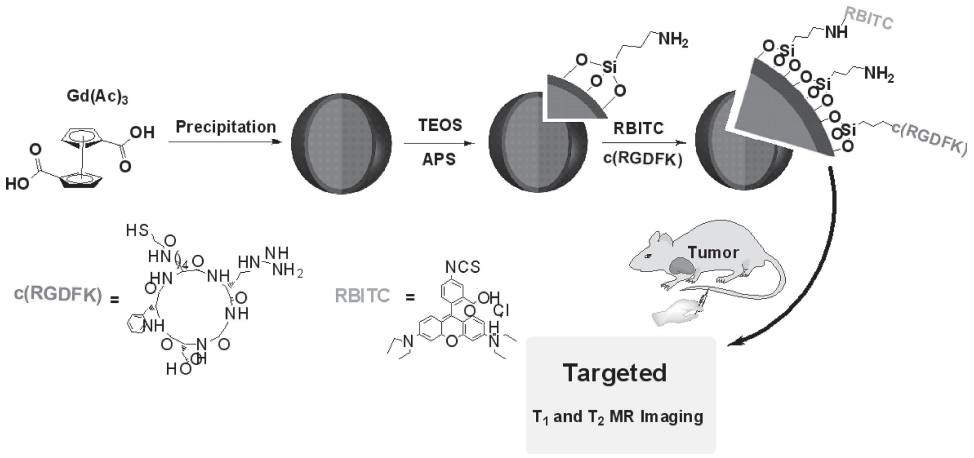

Scheme 1. Schematic illustration for targeted T_1- and T_2- weighted MR imaging of Fc-Gd@SiO_2(RBITC) –RGD NCPs.

interdisciplinary fields.[9] Recently, nanoscale coordination polymers (NCPs) have opened up a new avenue for biomedical applications due to their unique and highly tailorable properties. For example, Lin and co-workers[10] have reported gadolinium/manganese based NCPs with controllable morphologies for biomedical imaging and drug delivery. Horcajada and co-workers[11] published non-toxic porous iron(III)-based NCPs with engineered cores and surfaces to serve as nanocarriers for drug delivery and imaging applications. Our group[12] also developed magnetophosphorescent d-f NCPs formed by phosphorescent carboxyl-functionalized Ir(III) complexes as building blocks interconnected by magnetic Gd(III) ions for phosphorescence and MR imaging. In the present study, we develop Gd-based nanoscale coordination polymers (NCPs) for targeted dual-mode T_1- and T_2-weighted MR imaging on a single instrument in vivo. Firstly, stable Fc-Gd NCPs were synthesized by 1,1′-dicarboxyl ferrocene as building blocks and Gd(III) ions with highly paramagnetic properties as metallic nodes using a nanoprecipitation method. The silica-coated NCPs were aminated through silanization, which enabled further covalent conjugation of a fluorescent rhodamine dye (RBITC) and RGD peptide onto their surface (**Scheme 1**) for targeted imaging in vitro and in vivo. The formed Fc-Gd@SiO_2(RBITC)–RGD NCPs were characterized by transmission electron microscopy (TEM), scanning electron microscopy (SEM), Fourier transform infrared (FT-IR) spectroscopy and relaxivity measurements. The targeting specificity of Fc-Gd@SiO_2(RBITC)–RGD NCPs were evaluated by T_1- and T_2-weighted MR imaging in vivo. To the best of our knowledge, this is the first report on the fabrication of NCPs for targeted T_1- and T_2-weighted MR imaging of tumors in vivo.

2. Results and Discussion

2.1. Synthesis and Characterization of Silica-Coated Fc-Gd NCPs

Fc-Gd NCPs were synthesized by the reported nanoprecipitation method.[13] In a typical synthesis, 4.5 mL $Gd(Ac)_3$ (6.6 mM) aqueous solution was added into 30 mL ethanol solution of 1,1′-dicarboxyl ferrocene (1.0 mM). The mixture was stirred at room temperature for 9 h, and then NCPs were isolated by centrifugation and washed with ethanol. SEM and TEM showed Fc-Gd NCPs have a spherical shape with a diameter of ≈80 nm (**Figure 1**a1 and 1b1). Dynamic light scattering (DLS) in ethanol gives an average size of ≈83 nm (Figure S1), which is very similar to the size observed by SEM and TEM. The zeta potential of Fc-Gd NCPs is ≈18 mV (Figure S2), resulting in their high dispersivity in ethanol. No obvious diffraction peaks were observed from powder X-ray diffraction (PXRD) (Figure S3), indicating the amorphous structure of Fc-Gd NCPs. The carboxylate stretching frequencies located at 1538, 1492 and 1391 cm^{-1} in the FT-IR spectrum of Fc-Gd NPs (Figure S4) are comparable to those for a Gd-based ferrocenyl coordination polymer,[14] which suggests a similar metal carboxylate connectivity. Furthermore, Fe-Gd NCPs contains the nanopores with the diameter of ≈3.8 nm (Figure S5). Following our previously published procedure,[15] Fc-Gd NCPs were modified with silica treated by both tetraethyl orthosilicate and (3-aminopropyl)triethoxysilane to achieve water solubility and surface amination for further modification, which was confirmed by a strong broad band at ≈1058 cm^{-1} corresponding to the Si-O-Si asymmetric (ν_{as}) stretching vibration in the FT-IR spectrum of Fc-Gd@SiO_2 NCPs (Figure S4). SEM and TEM images showed Fc-Gd@SiO_2 NCPs have a diameter of ≈86 nm with a zeta potential of +22.7 mV (Figure S6). Their mean diameter determined by DLS is ≈116.3 nm (Figure S7) in aqueous media. The larger diameter than that observed by TEM is attributed to slight aggregation.

2.2. Functionalization of Fc-Gd@SiO_2 NCPs

To conveniently investigate the targeting ability of Fc-Gd@SiO_2 NCPs, a targeting ligand RGD and fluorescent dye (RBITC) were modified on the surface of the NCPs. The density of amine moieties on the surface of NCPs of ≈4.9×10^{-4} mol/g was firstly determined using the primary amine nitrogen kit.[16] Then RBITC was reacted with a portion of the primary amines of

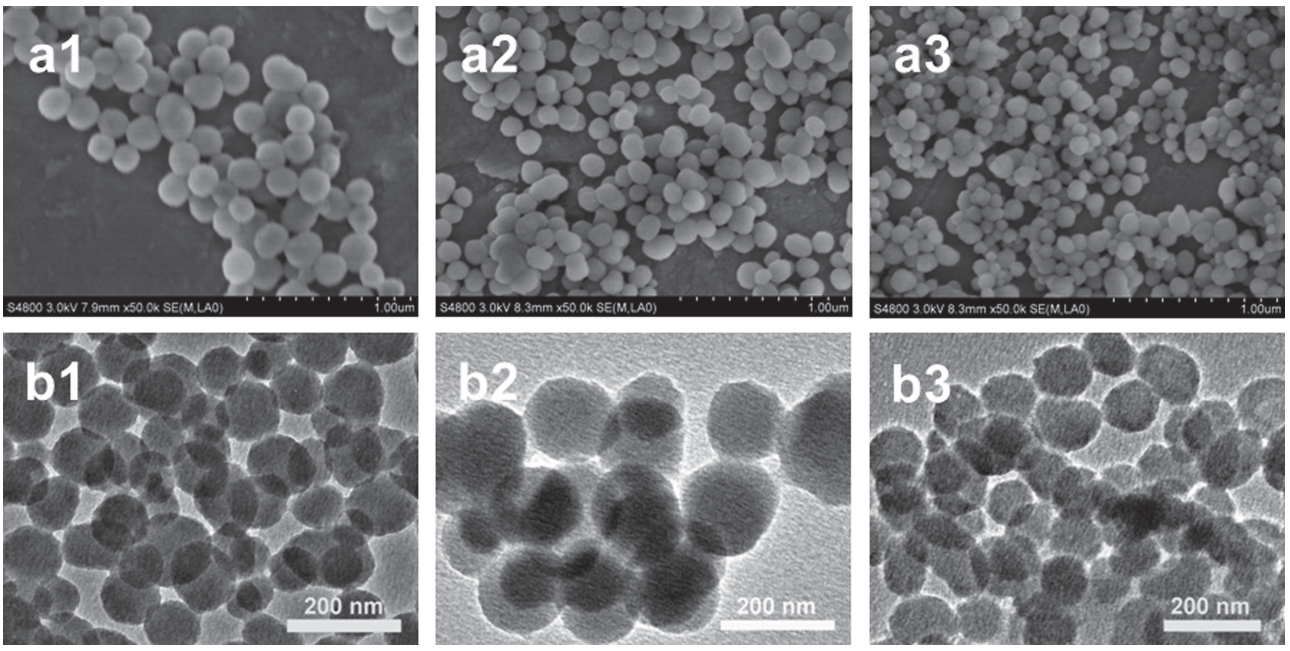

Figure 1. SEM images of Fc-Gd NCPs (a1), Fc-Gd@SiO_2 NCPs (a2), and Fc-Gd@SiO_2(RBITC)–RGD NCPs (a3); TEM images of Fc-Gd NCPs (b1), Fc-Gd@SiO_2 NCPs (b2), and Fc-Gd@SiO_2(RBITC)–RGD NCPs (b3).

Fc-Gd@SiO_2 NCPs via a thiourea linkage. The unreacted dyes were removed by dialysis. As a result, Fc-Gd@SiO_2(RBITC) NCPs with a diameter of ≈161.4 nm, measured by DLS (Figure S8), could be dispersed in water and exhibited the characteristic fluorescence of an RBITC dye (**Figure 2**). After the RBITC conjugation, the amount of the remaining amine groups of Fc-Gd@SiO_2(RBITC) NCPs available on the surface for further conjugation was quantified to be ≈1.9×10^{-4} mol/g. Accordingly, the surface potential of NCPs varied to +12.8 mV for Fc-Gd@SiO_2(RBITC) NCPs (Figure S9), which can be explained by the surface coverage of NCPs with an RBITC dye. Fc-Gd@SiO_2(RBITC) NCPs could be well dispersed in water and have a strong luminescence (Figure 2a). Thirdly, RGD was conjugated with Fc-Gd@SiO_2(RBITC) NCPs to perform their targeting capability. Fc-Gd@SiO_2(RBITC) NCPs were firstly maleimide-functionalized by reacting with a heterobifunctional cross-linker, 6-maleimidohexanoic acid *N*-hydroxysuccinimide ester, and then coupled with the thiolated c(RGDFK) to form RGD-conjugated NCPs. The peaks at 1659 cm^{-1} (amide I) resulting from the amide groups (Figure S4) indicated the formation of the polypeptide block.[17] TEM showed that Fc-Gd@SiO_2(RBITC)–RGD NCPs had the similar diameter of ≈95 nm to that of Fc-Gd@SiO_2 NCPs. The surface potential decreased to +10.9 mV for Fc-Gd@SiO_2(RBITC)–RGD NCPs (Figure S10). The hydrodynamic diameter was decreased to ≈99.4 nm (Figure S10), indicating that RGD moieties not only perform the targeting properties, but also improve the dispersivity in aqueous media of NCPs. To verify their stability under physiological conditions, the diameter changes of Fc-Gd@SiO_2(RBITC)–RGD NCPs were monitored in minimum essential medium (MEM) plus 10% fetal bovine serum (FBS) as simulated in vivo plasma. After 84 h, the size varied from ≈158.5 nm to ≈181.3 nm (Figure 2b). Furthermore, the silica shell stabilized Fc-Gd@SiO_2(RBITC)–RGD NCPs against dissolution. In MEM plus 10% FBS, only ≈2.0% free Gd ions were released from NCPs after 9 days, as measured by inductively coupled plasma mass spectrometry (ICP-MS) (Figure 2c), which is stable enough for in vivo application.

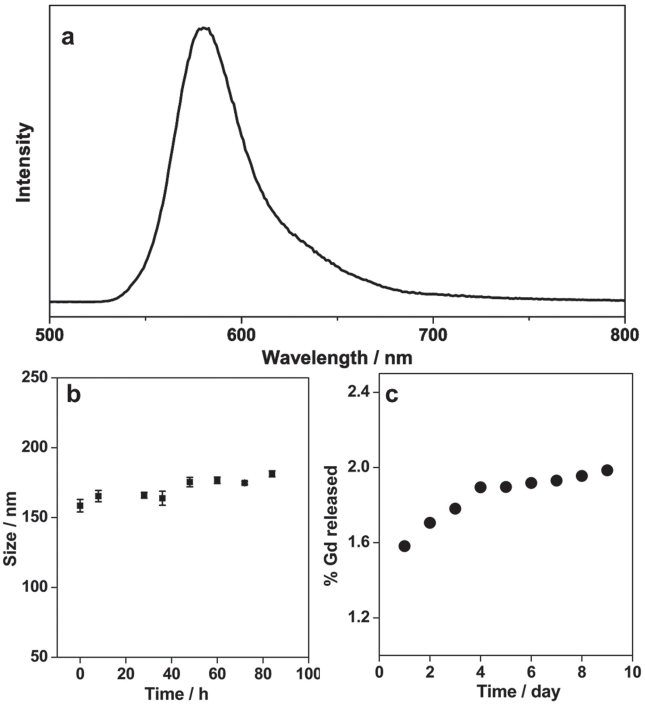

Figure 2. a) Fluorescence spectra of Fc-Gd@SiO_2(RBITC) NCPs in aqueous media under the 488 nm excitation. Hydrodynamic size changes (b) and release profile of Gd^{3+} ions (c) from Fc-Gd@SiO_2(RBITC)–RGD NC Ps incubated in MEM plus 10% FBS.

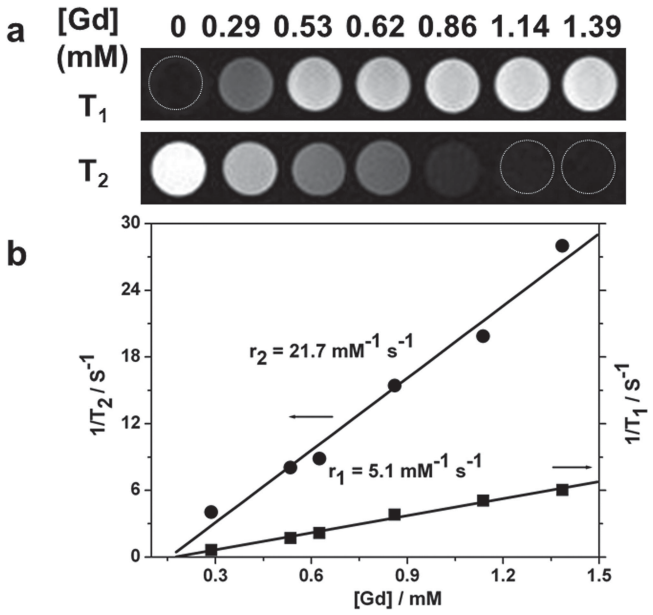

Figure 3. a) T_1 and T_2 MR images of Fc-Gd@SiO_2(RBITC)–RGD in water at 3.0 T MR system. The upper part of panel a shows the T_1 images, and the lower part of panel a shows the T_2 images. b) T_1 and T_2 relaxivity plot of aqueous suspension of Fc-Gd@SiO_2(RBITC)–RGD NCPs .

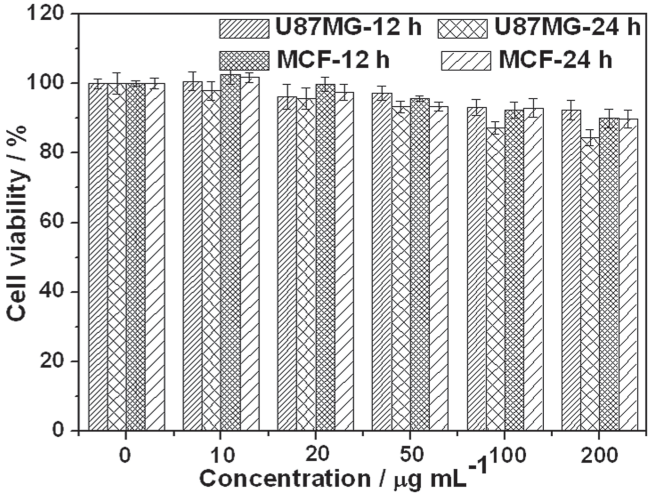

Figure 4. In vitro cell viability of U87MG and MCF-7 cells incubated with Fc-Gd@SiO_2(RBITC)–RGD NCPs with different concentrations incubated for 12 and 24 h at 37 °C.

2.3. Relaxivity Property of Fc-Gd@SiO_2(RBITC)–RGD NCPs

To validate the dual-mode MR imaging, the T_1- and T_2-weighted MR images were acquired with different concentrations of Gd ions, and the longitudinal (r_1) and transversal relaxivity (r_2) of Fc-Gd@SiO_2(RBITC)–RGD NCPs in aqueous media were measured using 3.0 T MR systems. As shown in **Figure 3**a, Fc-Gd@SiO_2(RBITC)–RGD NCPs display a signal enhancement in the T_1-weighted MR images with the increase of Gd concentration. The r_1 value was determined to be ≈5.1 mM^{-1} s^{-1} (Figure 3b). This value is consistent with that of the previously reported Gd-DTPA (r_1 = 4.8 mM^{-1} s^{-1}),[18] suggesting that NCPs have a similar T_1-positive contrast effect to that of Gd-DTPA. Likewise, the r_2 value was determined to be 21.7 mM^{-1} s^{-1} for the 3.0 T MR systems (Figure 3b), which is about four times higher than that of Gd-DTPA (r_2 = 5.3 mM^{-1} s^{-1}).[18] The impressive r_2 value of NCPs, which is ascribed to the combined effects of the local inhomogeneous magnetic fields created by magnetic NCPs and the exchange of water between NCPs and the bulk,[19] simultaneously resulted in an obvious signal reduction in the T_2-weighted MR images with increasing concentration of Gd ions (Figure 3a). The suitable r_2/r_1 ratio (r_2/r_1 = 4.3) indicated the potential use of Fc-Gd@SiO_2(RBITC)–RGD NCPs as a T_1/T_2 dual-mode contrast agent.

2.4. Cytotoxicity Assay

Prior to the applications of Fc-Gd@SiO_2(RBITC)–RGD NCPs for in vivo MR imaging, the in vitro cytotoxicity was evaluated in U87MG and MCF-7 cell lines by MTT assay. As shown in **Figure 4**, no significant cytotoxic response (cell viability > 90%) was detected at concentrations below 100 μg mL^{-1} after incubation for 12 and 24 h, respectively. Even at a concentration of 200 μg mL^{-1}, the viability of U87MG cells remained above 84%. There is no significant difference in the cell viability between the different cell lines. This indicates that Fc-Gd@SiO_2(RBITC)–RGD NCPs exhibit a low cytotoxicity within our experimental concentration range, which is essential for their use in further biological applications.

2.5. Targeting Properties Confirmed by Flow Cytometry and ICP-MS Analysis

To illustrate the targeting properties of Fc-Gd@SiO_2(RBITC)–RGD NCPs as a platform for cancer cells, the cellular uptake was quantitatively determined by the fluorescence intensity on flow cytometry and the amount of Gd ions per cells was also measured by ICP-MS analysis. As shown in **Figure 5** and Figures S12–S14, the fluorescence intensity of U87MG cells is weak at a concentration of Fc-Gd@SiO_2(RBITC)–RGD NCPs below 10 μg mL^{-1}, suggesting low cellular uptake. The cellular uptake determined by the fluorescence on flow cytometry increased rapidly from ≈57.0% to ≈91.3% as the concentration increased from 10 to 30 μg mL^{-1}. However, further increasing the concentration to 100 μg mL^{-1}, the fluorescence of U87MG cells was nearly saturated. Therefore, the concentration of Fc-Gd@SiO_2(RBITC)–RGD NCPs was selected as 30 μg mL^{-1} for further investigation.

To confirm the receptor-mediated cellular uptake of Fc-Gd@SiO_2(RBITC)–RGD NCPs in U87MG cells, the block, negative and temperature control experiments were conducted (Figure 5). For the block experiment, free RGD (30 μg mL^{-1}) was pre-incubated with U87MG cells before incubation with Fc-Gd@SiO_2(RBITC)–RGD NCPs, thereby limiting the cellular uptake of NCPs (≈38.3%). The uptake of Gd ions in U87MG cells was decreased to 1.7 ± 0.6 pg/cell from 8.3 ± 0.6 pg/cell incubated with only Fc-Gd@SiO_2(RBITC)–RGD NCPs. For the

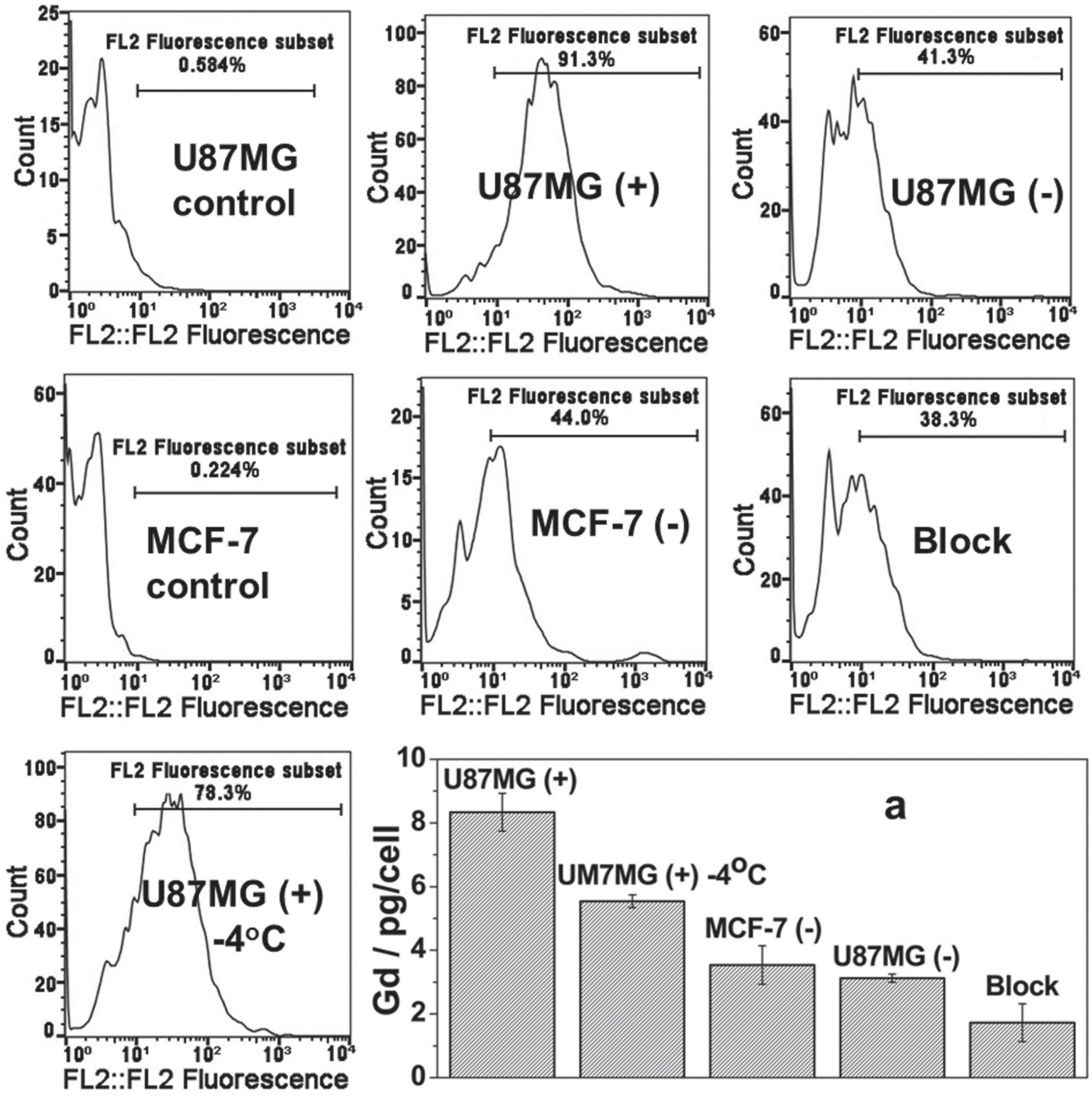

Figure 5. Flow cytometry profiles in different conditions. U87MG cells were incubated without (U87MG control), with Fc-Gd@SiO_2(RBITC)–RGD (U87MG (+)) and Fc-Gd@SiO_2(RBITC) NCPs in MEM at 37 °C (U87MG (-)), respectively; MCF-7 cells were incubated without (MCF-7 control) and with Fc-Gd@SiO_2(RBITC)–RGD NCPs (MCF-7 (-)) in DMEM at 37 °C, respectively; U87MG cells were preincubated with the free RGD (30 μg mL^{-1}) at 37 °C, and then incubated with Fc-Gd@SiO_2(RBITC)–RGD NCPs in MEM at 37 °C (block); U87MG cells were incubated with Fc-Gd@SiO_2(RBITC)–RGD NCPs in MEM at 4 °C (U87MG (+)-4°C). All the incubation concentration and time of NCPs are 30 μg mL^{-1} and 30 min, respectively. a: the uptake amount of Gd ions under different incubated condition.

negative control experiment, $\alpha_v\beta_3$ integrin-deficient MCF-7 cells were chosen. At 30 μg mL^{-1} Fc-Gd@SiO_2(RBITC)–RGD NCPs, relatively low cellular uptake of NCPs (≈44.0% determined by flow cytometry and 3.1 ± 0.1 pg/cell Gd ions measured by ICP-MS) was observed. As the incubation temperature decreased to 4 °C, the uptake of Fc-Gd@SiO_2(RBITC)–RGD NCPs in U87MG cells was ≈78.3%. Under the same incubation conditions, the uptake of Gd ions was 5.5 ± 0.2 pg/cell. These results indicated that the cellular uptake of Fc-Gd@SiO_2(RBITC)–RGD NCPs is mainly mediated by RGD endocytosis.

2.6. Targeted T_1- and T_2-weighted MR Imaging in Vitro

To confirm targeting ability of Fc-Gd@SiO_2(RBITC)–RGD NCPs for cancer cells by dual-mode MR imaging, both T_1- and

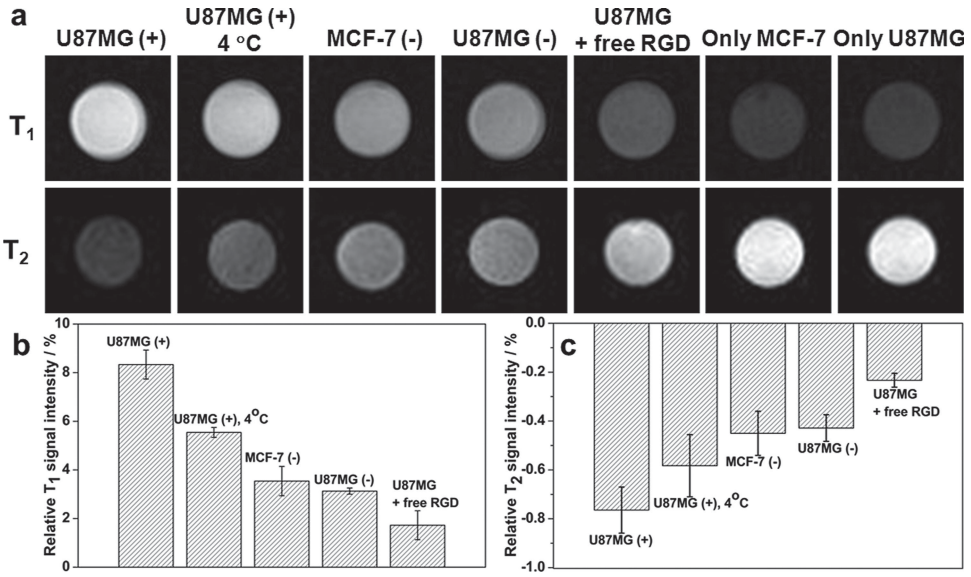

Figure 6. a) T_1- and T_2-weighted MR images of Fc-Gd@SiO_2(RBITC)–RGD NCPs on 3T MR system. U87MG (+): Fc-Gd@SiO_2(RBITC)–RGD NCPs in U87MG cells incubated at 37 °C; U87MG (+), 4 °C: Fc-Gd@SiO_2(RBITC)–RGD NCPs in U87MG cells incubated at 4 °C; MCF-7 (-): Fc-Gd@SiO_2(RBITC)–RGD NCPs in MCF-7 cells incubated at 37 °C; U87MG (-): Fc-Gd@SiO_2(RBITC) NCPs in U87MG cells incubated at 37 °C; U87MG + free RGD: Fc-Gd@SiO_2(RBITC)–RGD NCPs in free RGD-pretreated U87MG cells incubated at 37 °C; Only MCF-7 and only U87MG as controls; The relative signal intensity for T_1- (b) and T_2- (c) weighted MR images. All the incubation concentration and time of NCPs are 30 μg mL^{-1} and 30 min.

T_2-weighted MR images and the signal intensity of U87MG cells over-expressing $\alpha_v\beta_3$ integrin and MCF-7 cells deficient of $\alpha_v\beta_3$ integrin were collected after incubation with no targeted Fc-Gd@SiO_2(RBITC) and with targeted Fc-Gd@SiO_2(RBITC)–RGD NCPs (30 μg mL^{-1}) for 30 min. As shown in **Figure 6**, after incubation with targeted Fc-Gd@SiO_2(RBITC)–RGD NCPs, the T_1-weighted MR images showed a significant enhancement in U87MG cells, whereas the T_2-weighted MR images of the same cells showed a marked signal decrease. A quantitative analysis of the MR signal change also confirmed this point. When U87MG cells were incubated with Fc-Gd@SiO_2(RBITC)–RGD NCPs (30 μg mL^{-1}) for 30 min, the T_1-weighted MR signal intensity of U87MG cells was ≈8.3 times higher than that of control U87MG cells, and the T_2-weighted MR signal intensity was ≈80% lower than that of control U87MG cells. In sharp contrast, under the same condition, the T_1-weighted MR signal intensity of MCF-7 cells was only 2.6 times higher than that of control MCF-7 cells, and the T_2-weighted MR signal intensity decreased ≈45% compared with that of control MCF-7 cells. The significant difference between U87MG and MCF-7 cells in MR imaging is likely due to the specific cellular uptake of Fc-Gd@SiO_2(RBITC)–RGD NCPs into U87MG cells. To further prove that the specific binding and uptake of NCPs is mediated through the interaction between RGD and $\alpha_v\beta_3$ integrins that are over-expressed on the cell surface, a free RGD block experiment and temperature control experiment were designed. U87MG cells preincubated with the free RGD peptide (30 μg mL^{-1}) were then treated with Fc-Gd@SiO_2(RBITC)–RGD NCPs for 30 min. T_1- and T_2-weighted MR imaging data showed that the T_1-weighted MR signal intensity of U87MG cells was only about one times higher than that of the control cells, and T_2-weighted MR signal intensity decreased ≈23% compared with that of the control cells. In addition, U87MG cells were incubated with Fc-Gd@SiO_2(RBITC)–RGD NCPs at 4 °C in order to block the endocytosis process. Compared to that at 37 °C, the similar T_1- and T_2-weighted MR signal intensity in U87MG cells was observed (Figure 6b and c). Our results suggest that Fc-Gd@SiO_2(RBITC) –RGD NCPs can specifically affect both T_1- and T_2-weighted MR signals through $\alpha_v\beta_3$ integrin-mediated cellular binding and uptake.

2.7. Targeting Properties Confirmed by Laser Scanning Confocal Microscopy

The targeting properties of Fc-Gd@SiO_2(RBITC)–RGD NCPs were further investigated by laser scanning confocal microscopy (LSCM). After incubation with Fc-Gd@SiO_2(RBITC)–RGD NCPs (30 μg mL^{-1}) at 37 °C for 30 min, a strong fluorescence pattern was observed throughout the cytoplasm of U87MG cells over-expressing $\alpha_v\beta_3$ integrin (**Figure 7**a1 and a3) compared with that of $\alpha_v\beta_3$ integrin-deficient MCF-7 cells (Figure 7c1 and c3) under similar conditions. Compared to the non-targeted Fc-Gd@SiO_2(RBITC) NCPs (**Figure 8**d1 and d3), U87MG cells incubated with Fc-Gd@SiO_2(RBITC)–RGD NCPs exhibited stronger fluorescence, indicating higher cellular uptake of targeted NCPs. It is worth noting that the fluorescence is observed both on the surface and in the cytoplasm of U87MG cells, suggesting that a portion of NCPs is bound onto the cell surface and another portion of NCPs is internalized into cells through receptor-mediated binding and endocytosis. To further clarify the dominant receptor-mediated endocytosis mechanism of NCPs, U87MG cells preincubated with the free RGD (30 μg mL^{-1}) were then incubated with Fc-Gd@SiO_2(RBITC)–RGD NCPs for 30 min at 37 °C. As a result, negligible fluorescence was detected (Figure 7e1 and e3). Furthermore, a fluorescence

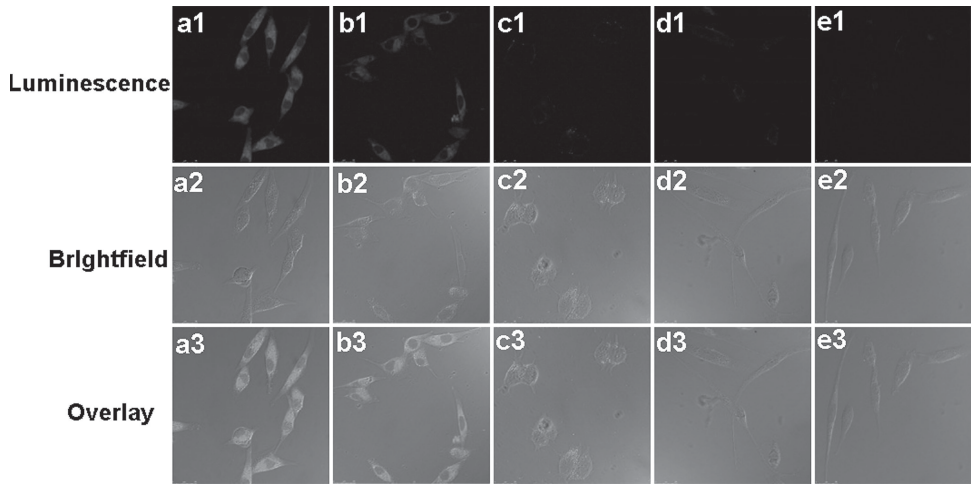

Figure 7. LCSM images of a1–a3) Fc-Gd@SiO_2(RBITC)–RGD NCPs in U87MG cells incubated at 37 °C; b1–b3) Fc-Gd@SiO_2(RBITC)–RGD NCPs in U87MG cells incubated at 4 °C; c1–c3) Fc-Gd@SiO_2(RBITC)–RGD NCPs in MCF-7 cells at 37 °C; d1–d3) Fc-Gd@SiO_2(RBITC) NCPs in U87MG cells incubated at 37 °C; e1–e3) Fc-Gd@SiO_2(RBITC)–RGD NCPs in free RGD-pretreated U87MG cells incubated at 37 °C. All the incubation concentration and time are 30 μg mL^{-1} and 30 min.

intensity in U87MG cells treated with Fc-Gd@SiO_2(RBITC)–RGD NCPs at 4 °C was similar to that at 37 °C (Figure 7b1 and b3). These results from LSCM images provide strong evidence that the binding and cellular uptake of Fc-Gd@SiO_2(RBITC)–RGD NCPs are dominantly mediated by RGD endocytosis.

2.8. Targeted T_1- and T_2-weighted MR Imaging in Vivo

The targeted dual-mode in vivo MR imaging for Fc-Gd@SiO_2(RBITC)–RGD NCPs was further performed with a 3 T MR imaging scanner. The T_1- and T_2-weighted MR images sequentially before and after intravenous injection of Fc-Gd@SiO_2(RBITC)–RGD NCPs (500 μL, 1 mg mL^{-1}) were acquired using a U87MG tumor xenograft mouse model. As a block experiment, the T_1- and T_2-weighted MR images sequentially before and after intravenous injection of both free RGD and Fc-Gd@SiO_2(RBITC)–RGD NCPs (500 μL, 1 mg mL^{-1}) were also acquired under similar experimental conditions. Compared with the pre-image, a bright T_1 signal enhancement from the T_1-weighted MR imaging was observed after 2 h post injection in the U87MG tumor. The boundary between the normal soft tissue and the tumor is clearly visible as shown in Figure 8a. More importantly, a T_2 signal decrease from the T_1-weighted MR imaging was simultaneously observed. The tumor was easy to be discriminated. The self-confirmed dual mode MR imaing shows the great potential use for accurate diagnosis of cancers. Figure 8b shows the change of the T_1 and T_2 signal intensity of the tumor in the targeted and block experiments. The T_1 signal intensity was enhanced 47 ± 5% in the targeted group whereas only 14 ± 3% enhancement was observed in the block groups. Accordingly, the T_2 signal intensity decreased 33 ± 5% in the targeted group whereas only 8 ± 1% enhancement was observed

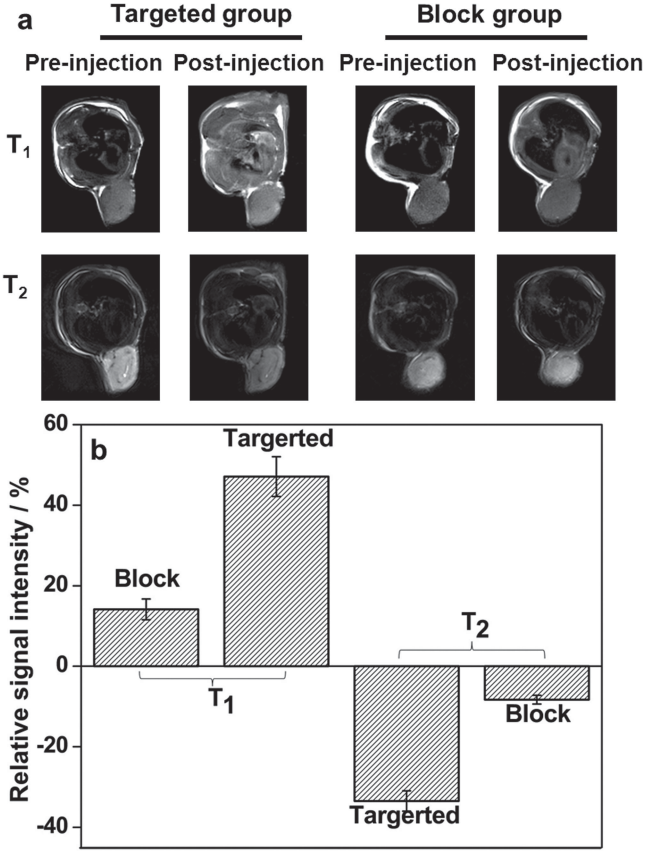

Figure 8. a) T_1-weighted and T_2-weighted MR images; b) signal intensity analysis of tumor. Targeted group: injected with Fc-Gd@SiO_2(RBITC)–RGD NCPs (500 μL,1 mg mL^{-1}); block group: injected with both free RGD and Fc-Gd@SiO_2(RBITC)–RGD NCPs (500 μL, 1 mg mL^{-1}).

in the block groups. Therefore, targeted Fc-Gd@SiO_2(RBITC)–RGD NCPs revealed excellent T_1- and T_2-weighted properties in vivo.

3. Conclusions

We developed unique Fc-Gd@SiO_2(RBITC)–RGD NCPs for dual-mode targeted T_1- and T_2-weighted MR imaging of cancer cells in vitro and in vivo. The formed multifunctional NCPs are water-dispersible, stable, and exhibit a low cytotoxicity at concentrations up to 200 μg mL^{-1}. The suitable r_2/r_1 ratio of the multifunctional NCPs enable dual-mode T_1- and T_2-weighted MR imaging of tumors in vivo. Our MR imaging data clearly indicate that the multifunctional Fc-Gd@SiO_2(RBITC)–RGD NCPs can specifically target cancer cells over-expressing $\alpha_v\beta_3$ integrin on the cell surface through a receptor-mediated delivery pathway. The T_1-weighted positive and T_2-weighted negative enhancement in the dual-mode MR imaging significantly improve the diagnosis accuracy. The developed Fc-Gd@SiO_2(RBITC)–RGD NCPs may conjugate with other biomolecules (e.g., antibodies, sugars, and peptides, etc.), thereby providing a versatile platform for targeting and dual-mode self-confirmed imaging of other biological systems.

4. Experimental Section

Materials: 1,1′-dicarboxyl ferrocene were purchased from J&K Chemical. Gadolinium acetate hydrate [$Gd(Ac)_3{\cdot}4H_2O$] and tetraethoxysilane (TEOS) were purchased from Sinopharm Chemical Reagent. Rhodamine B isothiocyanate (RBITC), 3-aminopropyltriethoxysilane (APS), *N*-hydroxysuccinimide (NHS), 3-(3-dimethylaminopropyl)-1-ethylcarbodiimide (EDC), and fetal bovine serum (FBS) were purchased from Sigma–Aldrich. 1-Ethyl-3-(3-dimethyllaminopropyl)carbodiimide hydrochloride were purchased from TCI. Thiolatedcyclo(Arg-Gly-Asp-Phe-Lys(mpa)) peptide (c(RGDFK)) were purchased from GL biochem(Shanghai) Ltd. All reagents were used without further purification. Water used in all experiments was purified using a Milli-Q Plus 185 water purification system (Millipore, Bedford, MA) with resistivity higher than 18 MΩ cm. Cellulose dialysis membranes (molecular weight cut-off, MWCO = 14 000) were acquired from Fisher.

Characterization Techniques: SEM images were recorded on a HitachS-4800 electron microscope operating at an accelerating voltage of 3.0 kV. TEM images were collected on a JEOL JEM-2010 transmission electron microscope operating at an accelerating voltage of 200 kV. FTIR spectra were collected using a Nicolet Avatar 370 FTIR spectrometer in the 400–4000 cm^{-1} region. The samples were pelletized with KBr before measurements. The surface potential andhydration radius weremeasured using a Malvern Zetasizer Nano ZS model ZEN3690 (Worcestershire, U.K.) equipped with a standard 633 nm laser. Fluorescence imaging was performed with a Leica TCS SP5 II inverted microscope with a Leica DMI 6000B confocal scanning system. All MR imaging measurements were performed Siemens Magnetom Trio with a 3.0 T systems. Flow Cytometry were analyzed with a Beckman Coulter flow cytometer (Quanta SC, USA). The concentration of Gd^{3+} ions was determined by inductively coupled plasma mass spectrometry (ICP-MS, VISTAMPXICP VARIAN).

Preparation of Fc-Gd@SiO_2 NCPs: Fc-Gd NCPs (10 mg) were dispersed in ethanol (20 mL) by sonication to form a well dispersed solution. Ammonium hydroxide (29.4%, 200 μL) was then added into the resulting mixture. After stirring for a while, TEOS (50 μL) was added dropwise to the reaction under vigorous stirring. The reaction was continued for 24 h at room temperature. The resulting Fc-Gd@SiO_2 NCPs were precipitated by centrifuged at 12 000 rpm for 15 min and washed three times with ethanol. Then, An ammonium hydroxide (29.4%, 80 μL) and APS (20 μL) was added separately to the above 20 mL ethanol solution of the collected Fc-Gd@SiO_2 NCPs, and subsequently the mixture was stirred at room temperature for further 12 h. The resulting NCPs were separated by centrifugation, washed three times with ethanol.

Preparation of Fc-Gd@SiO_2(RBITC) NCPs: Fc-Gd@SiO_2 NCPs (20 mg) were dissolved in tetrahydrofuran (THF, 100 mL), and RBITC (3 mg) was added to the above THF solution. The mixture was stirred at room temperature for 5 h, and the reaction was carried out under nitrogen atmosphere in dark without moisture. Lastly, the obtained Fc-Gd@SiO_2(RBITC)$_2$ NCPs were precipitated by centrifugation at 12 000 rpm for 15 min, and purified with ethanol by several cycles of redispersion and centrifugation.

Preparation of Fc-Gd@SiO_2(RBITC)-RGD NCPs: Fc-Gd@SiO_2(RBITC) NCPs (25 mg) was added to an ethanol solution (15 mL) containing the 6-maleimidohexanoic acid *N*-hydroxysuccinimide ester (2 mg) and 1-ethyl-3-(3-dimethyllaminopropyl)carbodiimide hydrochloride (2 mg). After 8 h at room temperature, the obtained NCPs were isolated via centrifugation, washed with ethanol three times. The precipitate was then redispersed into an ethanol solution (15 mL) containing c(RGDFK) peptide (6 mg), then gently stirred at room temperature for 12 h. The mixture was centrifuged and washed twice with ethanol. The precipitate was then redispersed into ethanol (5 mL) and placed inside a piece of dialysis membrane (MWCO 14 000) to remove the free RGD. The purified NCPs were resuspended in ethanol and stored at 4 °C before use.

Measurement of Release of Gd^{3+} Ions from Fc-Gd@SiO_2(RBITC)-RGD NCPs: 2.0 mL of a suspension of Fc-Gd@SiO_2(RBITC)-RGD NCPs in MEM with 10% FBS (2.55 mg) was placed inside a piece of dialysis membrane (MWCO 14 000). The dialysis membrane was submerged in 150 mL of MEM with 10% FBS under gentle stirring. Aliquots of the solution were then removed a different time points. 1 mL of 1 M nitric acid was added to the solution. The water was evaporated and the residue was redissolved in a 10 mL volumetric flask for ICP measurements.

Cell Culture: A human glioblastoma cell line (U87MG cells) and a human breast cancer cell line (MCF-7 cels) were provided by Shanghai Institutes of Biological Sciences (SIBS), Chinese Academy of Sciences (CAS, China). U87MG and MCF-7 Cells were cultured in MEM (Thermo, USA) and DMEM medium (Thermo, USA) supplemented with 10% FBS (Gibco, USA) and 1% penicillin-streptomycin solution (Thermo, USA) at 37 °C and 5% CO_2. Cells were generally plated in cell culture flask (Corning, USA) and allowed to adhere for 24 h, then harvested by treatment with 0.25% trypsin-EDTA solution (Gibco, USA).

In Vitro Cytotoxicity Assay: MTT assays were performed to evaluate the cytotoxicity of Fc-Gd@SiO_2(RBITC)-RGD NCPs at different concentrations and different time. U87MG and MCF-7 cells were plated at a density of 5×10^4 cells/well into 96-well plates for 24 h, followed by treatment with Fc-Gd@SiO_2(RBITC)-RGD NCPs at different concentrations (0, 10, 20, 50, 100, 200 μg mL^{-1} diluted in MEM and DMEM) for a further 12 or 24 h at 37 °C under 5% CO_2. Thereafter, thiazolyl blue tetrazolium bromide (MTT, 20 μL, 5 mg mL^{-1}) was added to each well and the plate was incubated for 4 h at 37 °C. Then, the supernatant was removed, and the formazan crystals were dissolved using DMSO (150 μL), followed by shaking at 150 rpm for 5 min. Finally, the optical absorption of formazan at 490 nm was measured by an enzyme-linked immunosorbent assay reader, with background subtraction at 690 nm was measured by microplate reader (Multiskan MK3, USA.).

Flow Cytometry: To determine the uptake contents of Fc-Gd@SiO_2(RBITC)-RGD NCPs, U87MG and MCF-7 cells were incubated with different concentrations (0, 3, 10, 30, and 100 μg mL^{-1}) of Fc-Gd@SiO_2(RBITC)-RGD NCPs in serum-free medium for 30 min after seeded in 6-well plates at 1×10^6 cells/well for 24 h. To confirm the receptor-mediated binding and endocytosis uptake of Fc-Gd@SiO_2(RBITC)-RGD NCPs by U87MG cells, U87MG cells were incubated with Fc-Gd@

SiO_2(RBITC) NCPs (30 μg mL^{-1}) and MCF-7 cells were incubated with Fc-Gd@SiO_2(RBITC)-RGD NCPs (30 μg mL^{-1}) for 30 min at 37 °C(negative control experiment). To block the endocytosis process, U87MG cells were incubated with Fc-Gd@SiO_2(RBITC)-RGD NCPs (30 μg mL^{-1}) for 30 min at 4 °C (temperature control experiment). To further confirm the dominant receptor-mediated endocytosis mechanism of NCPs, free RGD-pre-incubated (30 μg mL^{-1}) U87MG cells were then incubated with Fc-Gd@SiO_2(RBITC)-RGD NCPs (30 μg mL^{-1}) for 30 min at 37 °C (block experiment). Treated cells were then washed with PBS three times, and harvested by trypsinization. After the cells were spun-down, the cell pellet was washed once and resuspended with PBS, then analyzed with a flow cytometer. The collected data were analyzed by using WinMDI 2.9 software.

Laser Scanning Confocal Microscopy: U87MG and MCF-7 cells were plated for 24 h before the experiment in glass cover slips at 1.2×10^4 cell/cm^2. Then U87MG cells were incubated with Fc-Gd@SiO_2(RBITC)-RGD NCPs (30 μg mL^{-1}) for 30 min at 37 °C. To confirm the receptor-mediated binding uptake of Fc-Gd@SiO_2(RBITC)-RGD NCPs by U87MG cells, the block experiment, negative control experiment and temperature control experiment were investigated. After incubation, the alive cells were washed three times with PBS and visualized with serum-free medium. Fluorescence imaging was performed with an Leica DMI 6000B confocal scanning system. A 63× oil-immersion objective lens was used (Zoom: 1.4) under 22% Voltage. Excitation of RBITC was carried out with a tunable argon ion laser at λ = 488 nm, and emissions were collected in the wavelength range of 550–650 nm.

Relaxivity Measurements in Solution: We used aqueous solutions of various concentrations of Fc-Gd@SiO_2(RBITC)-RGD NCPs for T_1 and T_2 measurements. All MR imaging measurements were performed with a 3.0 T systems. T_1-weighted MR images were acquired using a conventional spin-echo sequence under the following parameters: TR/TE = 900/7.9 ms, 256 × 320 matrices, 128 × 128 mm field of view, 313 Hz/Px of bandwidth, a slice thickness of 3 mm. For T_2-weighted MR imaging, a fast spin-echo sequencewas used to reduce acquisition time with the same parameters of T_1-weighted MRI, except for TR/TE = 4000/284 ms and 220 Hz/Px of bandwidth.

T_1- and T_2-weighted MR Imaging in Cells: U87MG and MCF-7 cells were incubated with Fc-Gd@SiO_2(RBITC)-RGD NCPs suspension in cell culture medium for 30 min after seeded in 6-well plates at 1×10^6 cells per well for 24 h. U87MG cells were incubated with Fc-Gd@SiO_2(RBITC)-RGD NCPs (30 μg mL^{-1}) for 30 min at 37 °C. To confirm the receptor-mediated binding uptake of Fc-Gd@SiO_2(RBITC)-RGD NCPs by U87MG cells, the block experiment, negative control experiment and temperature control experiment were investigated. All MR imaging measurements were performed with a 3.0 T systems. T_1-weighted MR images were acquired using a conventional spin-echo sequence with the following parameters: TR/TE = 300/11 ms, 248 × 320 matrices, 124 × 160 mm field of view, 140 Hz/Px of bandwidth, a slice thickness of 3 mm. T_2-weighted MR images using a fast spin-echo sequence was used to reduce acquisition time under the following parameters: TR/TE = 6000/207 ms, 306 × 384 matrices, 127 × 159 mm field of view, 228 Hz/Px of bandwidth, and a slice thickness of 3 mm. The change of signal intensity in cells (%) = signal intensity of cells incubated with NCPs-signal intense of only cells)/ signal intensity of cells * 100%.

In vivo MR Imaging: To verify the dual-contrast ability of Fc-Gd@SiO_2(RBITC)-RGD NCPs for targeted imaging of a tumor model in vivo. U87MG cells were harvested by incubation with 0.05% trypsin-EDTA, after centrifugation and resuspension in 0.2 mL PBS, 2×10^6 cells were subcutaneously implanted into the left flank of each nude mouse, xenografted tumor reached 1.0–1.2 cm in diameter after ten days. A 500 μL of the Fc-Gd@SiO_2(RBITC)-RGD nanoparticles suspension (1 mg mL^{-1})with or without free RGD (1 mg mL^{-1}) was injected into nude mice through tail vein injection. In vivo MR imaging experiments were performed using a 3.0 T systems after injected for 2 h. T_1-weighted MR images were acquired using a conventional spin-echo sequence with the following parameters: TR/TE = 200/12 ms, 320 × 320 matrices, 60 × 60 mm field of view, 140 Hz/Px of bandwidth, a slice thickness of 1.5 mm. T_2-weighted MR images using a fast spin-echo sequence was used to reduce acquisition time under the following parameters: TR/TE = 6000/98 ms, 320 × 320 matrices, 60 × 60 mm field of view, 220 Hz/Px of bandwidth, and a slice thickness of 1.2 mm. Each in vivo scan was completed within half an hour. The change of signal intensity in tumor (%) = signal intensity of post-injection / signal intensity of pure water – signal intense of pre-injection / signal intensity of pure water * 100%.

Acknowledgements

This work was partially supported by National Natural Science Foundation of China (No. 21271130), program for Changjiang Schloars and Innovative Research Team in University (No. IRT1269), the Key Subject of Education Ministry of China (No. 210075), Shanghai Natural Science Fund Project (No. 12ZR1421800), Shanghai Municipal Education Commission (No. 13ZZ110) and Shanghai Normal University (Nos. DXL122, DYL20B05 and SK201339).

Received: July 19, 2013
Revised: August 13, 2013
Published online: October 25, 2013

[1] a) J. Cheon, J. H. Lee, *Acc. Chem. Res.* **2008**, *41*, 1630; b) S. H. Choi, H. B. Na, Y. I. Park, K. An, S. G. Kwon, Y. Jang, M. H. Park, J. Moon, J. S. Son, I. C. Song, W. K. Moon, T. Hyeon, *J. Am. Chem. Soc.* **2008**, *130*, 15573; c) M. Colombo, S. C. Romero, M. F. Casula, L. Gutierrez, M. P. Morales, I. B. Bohm, J. T. Heverhagen, D. Prosperi, W. J. Parak, *Chem. Soc. Rev.* **2012**, *41*, 4306; d) R. Hao, R. Xing, Z. Xu, Y. Hou, S. Gao, S. Sun, *Adv. Mater.* **2010**, *22*, 2729; e) J. Kim, Y. Piao, T. Hyeon, *Chem.Soc .Rev.* **2009**, *38*, 372.

[2] D. Yoo, J. H. Lee, T. H. Shin, J. Cheon, *Acc. Chem. Res.* **2011**, *44*, 863.

[3] a) P. Caravan, J. J. Ellison, T. J. McMurry, R. B. Lauffer, *Chem. Rev.* **1999**, *99*, 2293; b) B. H. Kim, N. Lee, H. Kim, K. An, Y. I. Park, Y. Choi, K. Shin, Y. Lee, S. G. Kwon, H. B. Na, J. G. Park, T. Y. Ahn, Y. W. Kim, W. K. Moon, S. H. Choi, T. Hyeon, *J. Am. Chem. Soc.* **2011**, *133*, 12624; c) H. Kloust, E. Poselt, S. Kappen, C. Schmidtke, A. Kornowski, W. Pauer, H. U. Moritz, H. Weller, *Langmuir* **2012**, *28*, 7276; d) H. B. Na, J. H. Lee, K. An, Y. I. Park, M. Park, I. S. Lee, D. H. Nam, S. T. Kim, S. H. Kim, S. W. Kim, K. H. Lim, K. S. Kim, S. O. Kim, T. Hyeon, *Angew. Chem. Int. Ed.* **2007**, *46*, 5397; e) J. Y. Park, M. J. Baek, E. S. Choi, S. Woo, J. H. Kim, T. J. Kim, J. C. Jung, K. S. Chae, Y. Chang, G. H. Lee, *ACS Nano* **2009**, *3*, 3663; f) U. I. Tromsdorf, O. T. Bruns, S. C. Salmen, U. Beisiegel, H. Weller, *Nano Lett.* **2009**, *9*, 4434.

[4] a) D. Ho, X. Sun, S. Sun, *Acc. Chem. Res.* **2011**, *44*, 875; b) E. Pöselt, H. Kloust, U. Tromsdorf, M. Janschel, C. Hahn, H. Weller, *ACS Nano* **2012**, *6*, 1619; c) K. E. Scarberry, E. B. Dickerson, J. F. McDonald, Z. J. Zhang, *J. Am. Chem. Soc.* **2008**, *130*, 10258; d) U. I. Tromsdorf, N. C. Bigall, M. G. Kaul, O. T. Bruns, M. S. Nikolic, B. Mollwitz, R. A. Sperling, R. Reimer, H. Hohenberg, W. J. Parak, S. Förster, U. Beisiegel, G. Adam, H. Weller, *Nano Lett.* **2007**, *7*, 2422; e) S. H. Wang, X. Shi, M. Van Antwerp, Z. Cao, S. D. Swanson, X. Bi, J. R. Baker, *Adv. Funct. Mater.* **2007**, *17*, 3043; f) H. Yang, C. Zhang, X. Shi, H. Hu, X. Du, Y. Fang, Y. Ma, H. Wu, S. Yang, *Biomaterials* **2010**, *31*, 3667; g) H. Yang, J. Zhang, Q. Tian, H. Hu, Y. Fang, H. Wu, S. Yang, *J. Magn. Magn. Mater.* **2010**, *322*, 973.

[5] K. H. Bae, Y. B. Kim, Y. Lee, J. Hwang, H. Park, T. G. Park, *Bioconjugate Chem.* **2010**, *21*, 505.

[6] H. Yang, Y. Zhuang, Y. Sun, A. Dai, X. Shi, D. Wu, F. Li, H. Hu, S. Yang, *Biomaterials* **2011**, *32*, 4584.

[7] Z. Li, P. W. Yi, Q. Sun, H. Lei, H. Li Zhao, Z. H. Zhu, S. C. Smith, M. B. Lan, G. Q. M. Lu, *Adv. Funct. Mater.* **2012**, *22*, 2387.
[8] Z. Zhou, D. Huang, J. Bao, Q. Chen, G. Liu, Z. Chen, X. Chen, J. Gao, *Adv. Mater.* **2012**, *24*, 6223.
[9] P. Horcajada, R. Gref, T. Baati, P. K. Allan, G. Maurin, P. Couvreur, G. Ferey, R. E. Morris, C. Serre, *Chem. Rev.* **2012**, *112*, 1232.
[10] a) J. Della Rocca, D. Liu, W. Lin, *Acc. Chem. Res.* **2011**, *44*, 957; b) R. C. Huxford, K. E. deKrafft, W. S. Boyle, D. Liu, W. Lin, *Chem. Sci.* **2012**, *3*, 198; c) W. Lin, W. J. Rieter, K. M. Taylor, *Angew. Chem. Int. Ed.* **2009**, *48*, 650; d) W. J. Rieter, K. M. Pott, K. M. L. Taylor, W. Lin, *J .Am. Chem. Soc.* **2008**, *130*, 11584; e) K. M. Taylor, A. Jin, W. Lin, *Angew. Chem. Int. Ed.* **2008**, *47*, 7722; f) K. M. L. Taylor, W. J. Rieter, W. Lin, *J. Am. Chem. Soc.* **2008**, *130*, 14358.
[11] P. Horcajada, T. Chalati, C. Serre, B. Gillet, C. Sebrie, T. Baati, J. F. Eubank, D. Heurtaux, P. Clayette, C. Kreuz, J.-S. Chang, Y. K. Hwang, V. Marsaud, P.-N. Bories, L. Cynober, S. Gil, G. Ferey, P. Couvreur, R. Gref, *Nat. Mater.* **2010**, *9*, 172.
[12] Z. Zhou, D. Li, H. Yang, Y. Zhu, S. Yang, *Dalton Trans.* **2011**, *40*, 11941.
[13] L. Qin, H. Yang, C. Qin, Z. Xiang, M. Zhang, L. Ding, T. Yi, S. Yang, *Dalton Trans.* **2013**, *42*, 4790.
[14] D. Guo, Y.-T. Li, C. Y. Duan, H. Mo, Q. J. Meng, *Inorg. Chem.* **2003**, *42*, 2519.
[15] H. Yang, Y. Zhuang, H. Hu, X. Du, C. Zhang, X. Shi, H. Wu, S. Yang, *Adv. Funct. Mater.* **2010**, *20*, 1733.
[16] B. C. Dukes, C. E. Butzke, *Am. J. Enol. Viticult.* **1998**, *49*, 125.
[17] C. Deng, H. Tian, P. Zhang, J. Sun, X. Chen, X. Jing, *Biomacromolecules* **2006**, *7*, 590.
[18] J. Lim, B. Turkbey, M. Bernardo, L. H. Bryant Jr., M. Garzoni, G. M. Pavan, T. Nakajima, P. L. Choyke, E. E. Simanek, H. Kobayashi, *Bioconjugate Chem.* **2012**, *23*, 2291.
[19] a) S. Aime, D. D. Castelli, S. G. Crich, E. Gianolio, E. Terreno, *Acc. Chem. Res.* **2009**, *42*, 822; b) N. Wartenberg, P. Fries, O. Raccurt, A. Guillermo, D. Imbert, M. Mazzanti, *Chem. Eur. J.* **2013**, *19*, 6980.